ACS APPLIED MATERIALS & INTERFACES

Research Article

www.acsami.org

Photocurrent Generation in Diamond Electrodes Modified with Reaction Centers

Roberta Caterino,[†] Réka Csiki,[†] Alina Lyuleeva,[†] Jonas Pfisterer,[†] Markus Wiesinger,[†] Stoffel D. Janssens,[‡] Ken Haenen,[‡] Anna Cattani-Scholz,[†] Martin Stutzmann,[†] and Jose A. Garrido*[,†]

[†]Walter Schottky Institut and Physik-Department, Technische Universität München, Am Coulombwall 4 Garching, 85748, Germany

[‡]Institute for Materials Research (IMO), Hasselt University & IMOMEC, IMEC vzw Wetenschapspark 1, 3590 Diepenbeek, Belgium

Supporting Information

ABSTRACT: Photoactive reaction centers (RCs) are protein complexes in bacteria able to convert sunlight into other forms of energy with a high quantum yield. The photostimulation of immobilized RCs on inorganic electrodes result in the generation of photocurrent that is of interest for biosolar cell applications. This paper reports on the use of novel electrodes based on functional conductive nanocrystalline diamond onto which bacterial RCs are immobilized. A three-dimensional conductive polymer scaffold grafted to the diamond electrodes enables efficient entrapment of photoreactive proteins. The electron transfer in these functional diamond electrodes is optimized through the use of a ferrocene-based electron mediator, which provides significant advantages such as a rapid electron transfer as well as high generated photocurrent. A detailed discussion of the generated photocurrent as a function of time, bias voltage, and mediators in solution unveils the mechanisms limiting the electron transfer in these functional electrodes. This work featuring diamond-based electrodes in biophotovoltaics offers general guidelines that can serve to improve the performance of similar devices based on different materials and geometries.

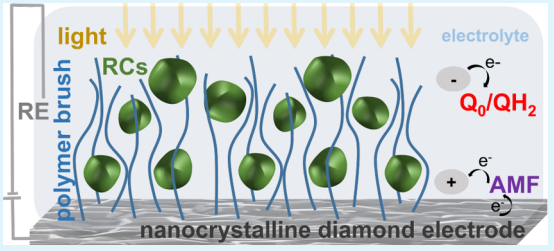

KEYWORDS: *diamonds, biophotovoltaics, reaction centers, surface functionalization, polymer brush, electron-transfer*

INTRODUCTION

Reaction centers (RCs) and photosystems (PSI and PSII) are the biological units enabling solar energy harvesting in plants and bacteria. The high efficiency of these species in achieving charge separation under photoexcitation, a result of billions of years of evolution, has attracted interest in using purified RCs, PSI, and PSII as a functional components in biosolar cells.[1−16] However, the complexity of the charge transfer between the biological species and the inorganic electrode typically leads to low values of the measured photocurrent in such systems with respect to traditional photovoltaics.[17] Despite its complexity, the RCs from purple bacteria have been isolated and extensively characterized in the last 20 years.[18−20] Many studies have shown that the protein is stable, robust, and capable of triggering a photostimulated electron transfer chain.[21,22]

Great effort has been devoted to optimize the immobilization of RCs on several surfaces making use of suitable linker molecules to prevent denaturation of the proteins in direct contact with the electrode surface.[23−26] Here we propose an innovative design to realize biophotovoltaic hybrid systems based on diamond, alternatively to metal electrodes, as it exhibits excellent electrochemical properties and, at the same time, it has the prerogative of providing a suitable surface for covalent immobilization of molecules and biomolecules of different nature.[27,28] Taking advantage of diamond versatility, we exploit two different surface functionalization methods established in recent works on oxidized diamond involving both self-assembled monolayers (ML)[29] as well as polymer brushes.[30,31] With the combination of functionalized diamond electrodes and the use of redox species in solution not yet exploited for these systems, we achieve a level of photocurrent density competitive with the results presented in literature so far for similar systems,[4,9,23,24,32] providing a new perspective for the research in this field.

To complete the picture, the understanding of some features of the photoresponse in RCs-based hybrid systems like the time dependence of the photocurrent in the presence of different mediators has been clarified, providing the equations, based on the classical theory of electrochemistry, which describe the relevant charge transfer mechanisms.

With the help of Figure 1, we discuss the details of the design and the electronic structure of the different building blocks constituting the biohybrid system. Here, we propose two designs, depicted in Figure 1a, based on RCs from *Rhodobacter spheroides* immobilized on diamond electrodes. In one design, the electrode is modified with a monolayer of 6-phosphono-hexanoic acid (see top of Figure 1b). In the other design, the diamond electrode is modified with poly(*tert*-butyl methyl

Received: January 23, 2015
Accepted: April 3, 2015
Published: April 3, 2015

ACS Publications © 2015 American Chemical Society

DOI: 10.1021/acsami.5b00711
ACS Appl. Mater. Interfaces 2015, 7, 8099−8107

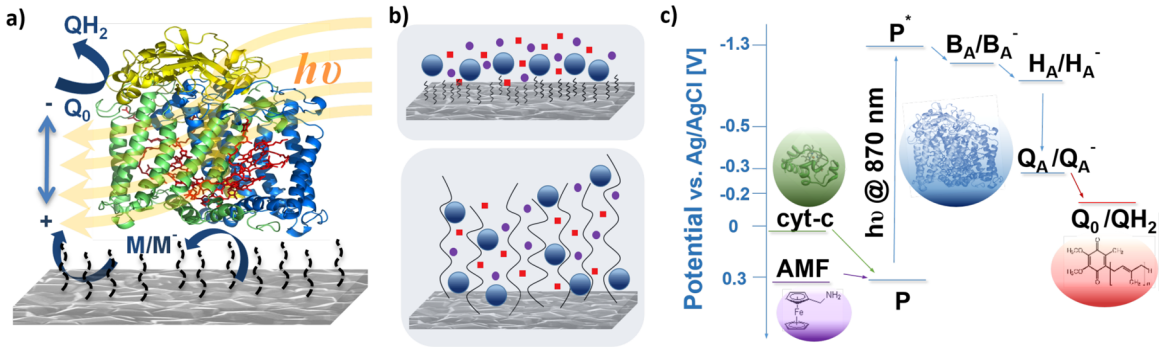

Figure 1. (a) Hybrid system consisting of RCs immobilized on a modified diamond electrode showing the different electron transfer processes involved in the photocurrent generation. An electron−hole pair is generated in the RCs under photostimulation. The high energy electron is extracted by a free quinone molecule (Q_0/QH_2 redox pair) and a low energy electron is provided by an electron mediator (M/M^- redox pair). (b) Schematic view of diamond electrodes modified with self-assembled monolayers (top) and polymers (bottom). The big blue spheres represent the RCs on the organic layers, and the red squares and the purple dots are Q_0 and AMF in solution, respectively. (c) Energy levels of the biohybrid system with respect to a Ag/AgCl electrode. The color code is the same as described above; in addition, green represents the electron mediator cytochrome *c*. The blue states belong to the RCs, where the high energy electron excited by the light relaxes stepwise through the internal states B_A/B_A^- and H_A/H_A^- and through the internal quinone Q_A/Q_A^- before being available for the reduction of Q_0 in solution.

acrylate) (PtBuMA) polymer brushes (see bottom of Figure 1b). The two differently modified electrodes have been investigated and their effects on the efficiency and the stability of the hybrid system are reported in this work. In particular, we will demonstrate that the diamond electrodes modified with the polymer PtBuMA enable a very high loading of redox molecules whereas the 6-phosphonohexanoic acid monolayer offers stability and fast charge transfer. In Figure 1c the energy levels of the different species involved in the photocurrent generation are shown. The oxidation and reduction potentials of the RCs have been established through a wide variety of spectroscopies; the values taken from the literature[33] are reported in Figure 1c and refer to the potential of the Ag/AgCl electrode used in the experiments presented in this work. Under exposure to light with a wavelength of 870 nm, one electron is excited from the state P to the P* of the RCs. The electron relaxes stepwise through the internal states B_A/B_A^- and H_A/H_A^- and through the internal quinone Q_A of the protein and is available to be extracted and released into the electrolyte. This task is enabled by ubiquinone Q_0 (2,3-dimethoxy-5-methyl-1,4-benzoquinone) in the solution, which is converted through the reaction with two photoelectrons into its reduced form, the dihydroquinone QH_2. In order to ensure the regeneration of the RCs, a low energy electron has to be injected from the electrode to the state P, to make it available for a new photoexcitation. The direct injection of the electrons from the electrode to the state P is not expected to be very efficient[32] so that an electron mediator in solution might be required.

Mimicking the natural operational environment[33] of the RCs, the protein cytochrome *c* (cyt-c) has been chosen as the first candidate to shuttle the low energy electron to the P state. This small heme protein is supposed to play in this system a role similar to the one it has in the photosynthetic membrane within the electron transport chain. As will be shown, cyt-c has certain disadvantages as electron mediator. In order to overcome the limitations of cyt-c, we propose the use of aminomethylferrocene (AMF) as a new mediator. This small and robust redox molecule of the family of ferrocenes will be shown to improve the charge transfer between the electrode and the RCs.

EXPERIMENTAL PROCEDURES

RCs from purple bacteria have been purchased isolated and purified from FRIZ Biochem Gesellschaft für Bioanalytik GmbH, Neuried, Germany and stored in TRIS buffer 10 mM pH 8 with 0.1% *N,N*-dimethyldodecylamine *N*-oxide (LDAO) at −25 °C. All other chemicals were purchased from Sigma-Aldrich.

Diamond Growth. Highly boron-doped nanocrystalline diamond (B-doped NCD) films were grown on Si as reported before.[34,35] Diamond growth was performed in an ASTeX 6500 series microwave plasma-enhanced chemical vapor deposition reactor. Growth conditions were optimized to produce a 150-nm-thick B-doped NCD layer with resistivity values of 10−50 mΩ·cm.[36]

Diamond Functionalization with a Monolayer of Organophosphonates. B-doped NCD substrates have been functionalized through the tethering per aggregation and growth (T-BAG method) following the protocol described in another work.[29] This procedure results in a monolayer of 6-phosphonohexanoic acid on the surface. The standard activation through EDC and Sulfo-NHS[37] enables the formation of peptide bonds with AMF and cytochrome *c*; details are also reported in the Supporting Information.

Grafting of Polymer Brushes on P-Type Doped NCD. The OH-terminated substrates are placed in a dry reaction quartz tube and heated in vacuum to 150 °C for 2 min, cooled down to room temperature, and put under argon protective atmosphere. tBMA is syringed into the reaction tube and degassed in liquid nitrogen. The setup is irradiated with UV light (λ = 350 nm) for 8 h. After irradiation, the samples are taken out of the reaction tubes and cleaned by ultrasonication in dichloromethane, ethyl acetate, and ethanol for 5 min, respectively. The chemical binding step (described in the next section) is based on amide bond formation between the amine group of cyt-c or AMF and an accessible carboxyl group on the macromolecular linker. Carboxyl groups can easily be obtained through saponification of *tert*-butyl methacrylate parts of the chain to PMAA.

Covalent Grafting of AMF and Cyt-c. Both procedures described above provide carboxyl-groups to serve as anchors for the covalent grafting of aminomethyl ferrocene (AMF) and cyt-c via amide bond. The standard activation of the carboxyl-group through EDC and Sulfo-NHS[37] enables the formation of amide bonds with AMF and cyt-c. The details of the functionalization procedure, passivation, and cleaning steps are reported in the Supporting Information.

Physisorption of RCs on the Functionalized Diamond Electrodes. After the covalent immobilization of the redox species AMF or cyt-c (also present in solution during the measurements) one can proceed with the physisorption of the RCs. RCs from purple bacteria have been stored in TRIS buffer 10 mM pH 8 with 0.1% *N,N*-

DOI: 10.1021/acsami.5b00711
ACS Appl. Mater. Interfaces 2015, 7, 8099−8107

dimethyldodecylamine *N*-oxide (LDAO) at −25 °C. The samples are covered with a drop of this solution diluted to 0.1 mg/mL of RC in buffer for 12−18 h in the dark at 4 °C. After this exposure, the sample is gently rinsed with DI water and measured immediately without exposure to direct light.

Electrochemical and Photoelectrochemical Characterization. The electrochemical characterization was performed in a three electrode electrochemical cell with a Gamry ref 600 potentiostat. A commercial Ag/AgCl was used as reference electrode (DriRef-5SH from World Precision Instruments, 3 M KCl, 210 mV against standard hydrogen electrode) and a Pt wire as counter electrode. The buffer used for the electrochemical measurements, when not differently specified, is a phosphate buffer solution (PBS) with an ionic strength of 10 mM (corresponding to a concentration of 3.5 mM) at pH 8.

RESULTS AND DISCUSSION

Sample Preparation and Electrochemical Characterization. Electrodes based on nanocrystalline diamond (NCD) were fabricated and functionalized according to the procedures described in the Experimental Section. In short, the NCD electrodes are covalently modified with either a monolayer (ML) of 6-phosphonoheaxoic acid or with a polymer brush (PtBuMA). Both linkers offer carboxyl groups to bind AMF or cyt-c via amide bonds. In the next step we have studied the efficiency of the charge transfer between these two type of electrodes and the species in solution which assist the photocurrent generation in our biophotovoltaic devices, i.e., AMF and cyt-c. The formal potential of cyt-c and AMF in solution were measured at +30 mV and +320 mV vs Ag/AgCl, respectively, as depicted in Figure 1c. A detailed discussion of the electrochemical characterization is provided in the Supporting Information. In short, our study evidences that AMF in solution enables a much faster electron transfer with diamond electrodes. In particular, the electron transfer rate constant for AMF in solution is $k_{AMF} = (0.06 \pm 0.02)$ cm s^{-1} consistent with literature values[38] and 1 order of magnitude higher than the one for cyt-c, $k_{cyt\text{-}c} = (0.006 \pm 0.002)$ cm s^{-1}. As discussed in the next section, this difference has a major impact on the performance of the biohybrid devices.

The preparation of the photoreactive hybrid systems is completed by the physisorption of the RCs on the diamond electrodes. For the electrodes modified with the monolayer, two kind of samples have been investigated: one prepared by covalently binding the cyt-c to the monolayer and the other by attaching AMF (details on the functionalization are provided in the Experimental Section). The RCs have been physisorbed on the differently prepared electrodes, which were then measured in a buffer solution containing 100 μM of Q_0 and the corresponding mediator (cyt-c or AMF). Since the RCs are most likely randomly oriented after physisorption, the attachment of the mediators to the electrode surfaces might help to achieve an efficient charge transfer to the RCs oriented with their P-side facing the surface.

Photocurrent Enhancement. In order to increase the generated photocurrent and improve the performance of the biophotovoltaic device, we propose the use of AMF as alternative to cyt-c as charge shuttle in solution. The role of the mediators in the generation of the photocurrent is presented in this section based on the experiments carried out in different solutions.

In addition, the effect of the electrode surface modification with monolayer or with a polymer brush on the photocurrent intensity is presented. Considering that an increased RCs loading should result in a higher photocurrent, we propose a 3D structured electrode where the polymer brush serves as a scaffold to entrap the photosynthetic proteins on the surface.

Figure 2a shows chronoamperometry measurements performed in a sample modified with the monolayer at a constant

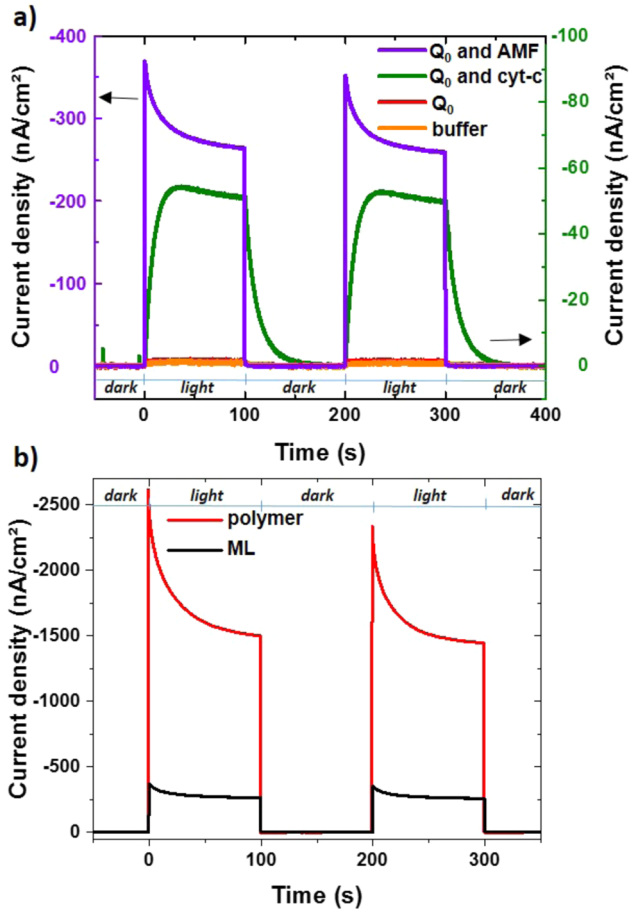

Figure 2. (a) Chronoamperometry under light exposure (0−100 s and 200−300 s) interrupted by time intervals in the dark (100−200 s, before 0 and after 300 s). The curves correspond to the samples modified with a monolayer and RCs in pure 10 mM PBS buffer (orange curve), with the addition of 100 μM Q_0 (red curve), with Q_0 and 10 μM cyt-c (green curve), with Q_0 and 200 μM AMF (purple curve); all curves recorded with $U_{bias} = -100$ mV. (b) Photocurrent density measured in chronoamperometry under periodical light exposure for a diamond electrode modified with the ML (black curve) and an electrode modified with a polymer brush (red curve). The experiments were performed in a buffer solution containing 100 μM Q_0 and 200 μM AMF.

potential of $U_{bias} = -100$ mV applied to the working electrode with respect to the Ag/AgCl reference electrode under photostimulation, in which the sample is exposed to IR light (LED at 870 nm) for 100 s, followed by 100 s in the dark. The sequence was repeated two times. No significant response to light was observed when measuring in pure buffer (orange curve) or in the presence of only Q_0 in the solution (red curve).

As discussed above, both mediators are necessary in solution to close the charge transfer cycle and observe a photocurrent. An optimized value for the concentration of the mediators was determined by a systematic study of their influence on the photocurrent (more details in the Supporting Information). To prove that the RCs are responsible for the observed photocurrent, the sample was intentionally treated with a

DOI: 10.1021/acsami.5b00711
ACS Appl. Mater. Interfaces 2015, 7, 8099−8107

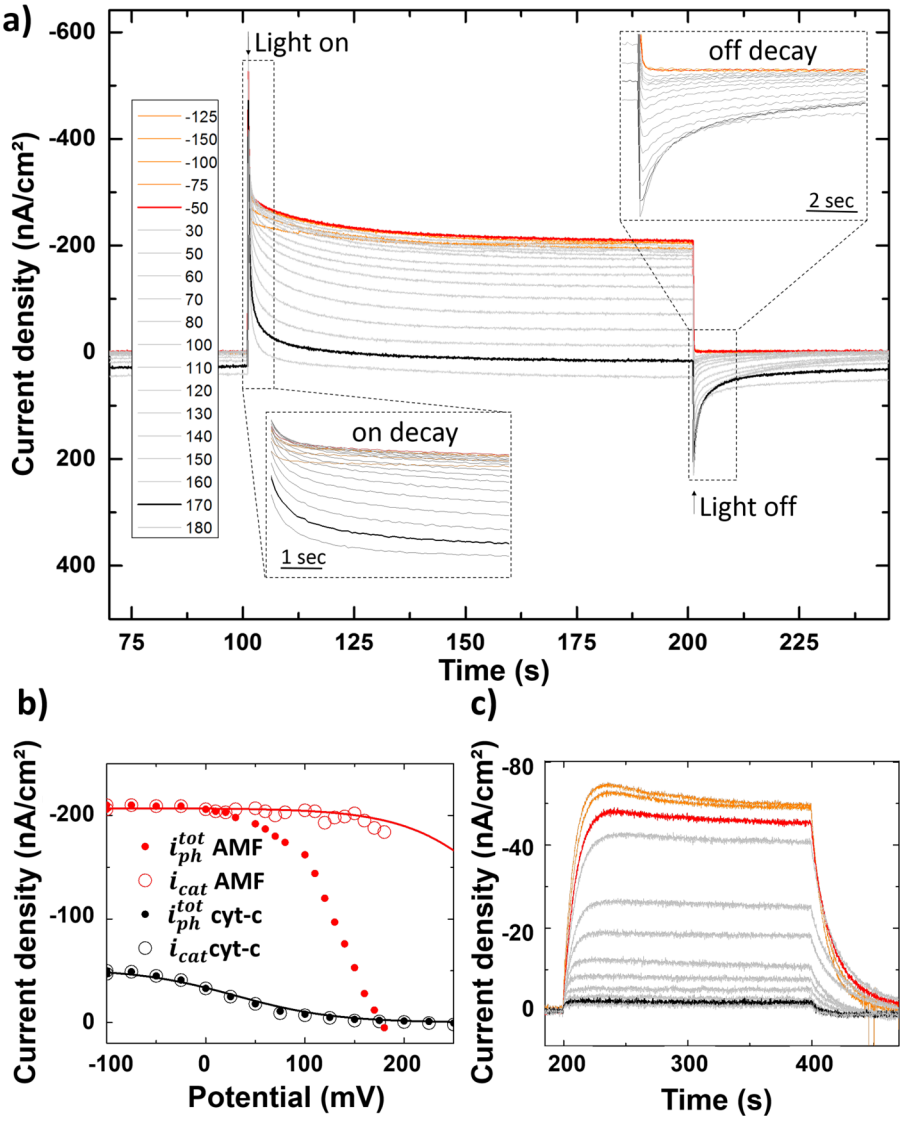

Figure 3. (a) Photocurrent curves recorded at different electrode bias (given in mV) for the case of AMF electron mediators. The insets provide a zoom into (i) the first seconds of the current decay after the light is switched on (bottom left), referred to as on decay, and (ii) the time response after switching off the light (up right), referred to as off decay. (b) Saturation current as a function of the bias voltage for samples with AMF (red) and cytochrome *c* (black) in solution. The solid symbols represent $i_{ph}^{tot}(t_{OFF}^{-})$, i.e., the saturation current calculated from the curves reported in part a right before switching off the light (t_{OFF}^{-}) with respect to the initial value of dark current. The open symbols represent $i_{cat}(t_{OFF}^{-})$, i.e., the cathodic current obtained after the correction described in the text. The solid lines represent fits using a diffusion-limited current−voltage dependence. (c) Photocurrent curves for the case of cyt-c as electron mediator.

concentrated solution of sodium dodecyl sulfate (SDS), a surfactant known to cause protein denaturation. As expected, the photocurrent signal disappeared after the treatment (measurements are shown in the Supporting Information).

Figure 2a also compares the chronoamperometry experiments performed with electrodes using either AMF (purple curve) or cyt-c (green curve) as electron mediators. As the figure reveals, the response to light is much faster for the system with AMF: after an initial rapid increase, the photocurrent decays to a value above 250 nA cm^{-2}, which is about five times higher than the value obtained for the electrode using cyt-c as the electron mediator (below 50 nA cm^{-2}). Further, for the cyt-c electron mediator, a very slow response is observed both when the light is switched on and when is switched off. The observed remarkable differences of the photocurrent response when using these two electron mediators are consistent with our observation that AMF exhibits a much higher charge transfer efficiency with diamond electrodes than cyt-c, evidenced by the differences in the heterogeneous rate constants calculated above. The more efficient charge transfer between AMF and the diamond electrode results in an improved injection of the low energy electron to the P state of the RCs.

In addition to the charge transfer efficiency, another relevant aspect which influences the photocurrent value is the density of RCs that can be "electrically contacted" on the surface of the electrodes. Whereas monolayers of RCs very close to the surface can exhibit an enhanced charge transfer to the electrode, multilayers of RCs trapped on conductive scaffolds can yield high photocurrents provided that the electron exchange with the electrode is fast enough. To investigate this issue, we have physisorbed RCs on diamond electrodes modified with a polymer brush functionalized with redox molecules (see Experimental Section for details on the surface-initiated

DOI: 10.1021/acsami.5b00711
ACS Appl. Mater. Interfaces 2015, 7, 8099−8107

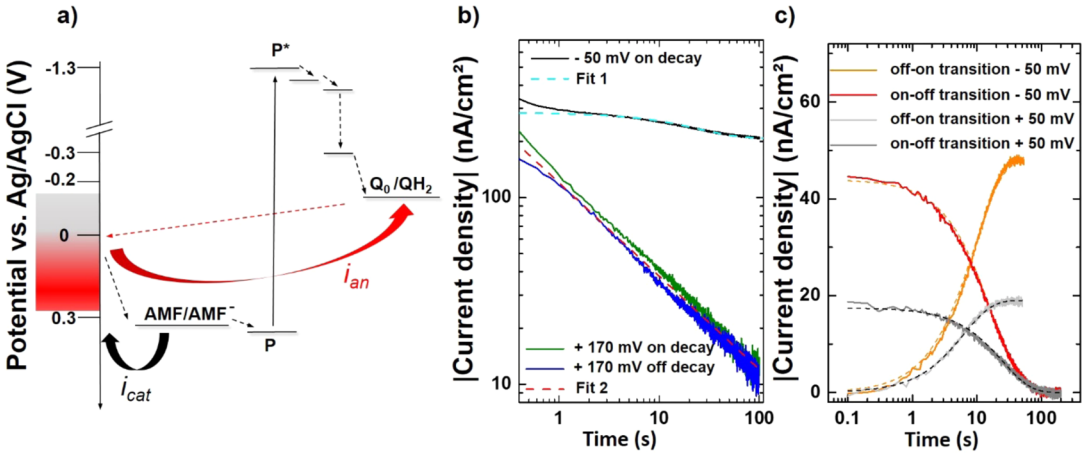

Figure 4. (a) Energy diagram (vs Ag/AgCl electrode). The dashed arrows indicate electron transfer processes at the electrode and the solid curved arrows the corresponding currents. Red color indicates the voltage regime of bias potential which favors anodic current. The gray area indicates the potential range at which only cathodic current (black arrows) is observed. (b) Absolute value of current density versus time and corresponding fit for the data shown in Figure 3a. The black curve represents the on decay at −50 mV, and the green curve the on decay at +170 mV. The curve in blue represents the experimental data for the off decay observed at positive bias voltages, i.e., the decay of i_{an} after the light is switched off. The equations used to fit the experimental data (dashed lines) are described in the text. (c) On−off current transition (dark red and dark gray curves) and off−on current transition (light red and light gray) for the case of cyt-c in solution. As representative examples, the experimental curves recorded at +50 mV (gray curves) and −50 mV (red curves) and the corresponding fits are shown.

polymer grafting). Figure 2b compares the photoresponse of a diamond electrode with RCs confined on a monolayer of 6-phosphonohexanoic acid molecules (black curve) and that of an electrode with RCs trapped on a PtBuMA polymer brush (red curve). After the initial decay, the current density for the polymer-modified electrode reaches a value close to 1.5 μA cm^{-2}. This is three times higher than the photocurrent measured with the electrode modified with a monolayer and superior to typical values of photocurrent density (20−400 nA cm^{-2}) reported in the literature for biohybrid photovoltaics systems based on one monolayer of RCs confined on gold electrodes[4,9,23,32,39] or carbon nanotubes.[6,24] The measured photocurrent transitions when light is switched on and off are both very fast for these two electrodes. The main effect of the polymer brush is an enhanced photocurrent, enabled by the capability of the polymer brushes to load more photoreactive proteins. It is worth recalling here that the electrochemical characterization of the polymer-modified electrodes (see Supporting Information) revealed a very high loading of ferrocene molecules into the polymer matrix. In the case of the RCs, of much larger dimensions than ferrocene, a lower loading is to be expected. Still, the high loading of RCs into the polymer-modified diamond electrodes is demonstrated by the considerably larger photocurrent signal measured for these electrodes compared to the case of RCs on SAM-modified electrodes.

Electron Transfer Mechanisms Voltage and Time Dependence of Photocurrent. In order to understand the mechanisms limiting the electron transfer in these biofunctional diamond electrodes, we will first discuss the dependence of the photocurrent on the bias voltage applied to the diamond electrodes. Figure 3a shows photocurrent curves measured (with Q_0 and AMF in solution) in the chronoamperometric mode as a function of the applied voltage for RCs immobilized on a sample functionalized with a monolayer of organo-phosphonates.

The arrows indicate the time when the light is switched on and off. The two insets in Figure 3a show the transitions of the current right after the light is switched on (left inset) and off (right inset). To facilitate the discussion, we make the following definitions for the photocurrent time responses. The increase (decrease) of the current after the light is switched on (off) is referred to as off−on (on−off) transition. The drop of the photocurrent during illumination is referred to as "on decay" (represented in the lower left inset in Figure 3a). The current response observed in the positive voltage regime after the light is switched off (presented in the upper right inset in Figure 3a) is referred to as "off decay". The curve highlighted in red corresponds to the experiment at −50 mV (vs Ag/AgCl) and is taken as an example of the behavior in the negative voltage regime, to which the other orange curves also belong. In the negative bias regime, the experiment with AMF mediators in solution exhibits a very fast response to photostimulation. In addition, the photocurrent decays considerably during illumination. After switching the light off, the signal goes rapidly back to the initial value. In this voltage range, the photocurrent transitions to the on state (off−on transition) and to the off state (on−off transition) are too fast to be resolved with our setup. This behavior changes in the positive voltage regime, as evidenced by the gray curves in Figure 3a. The curve highlighted in black was recorded at a bias voltage of +170 mV, and will be used as a representative example of the electrode response in this bias regime. The photocurrent decay during illumination (on decay) becomes more important for more positive potentials. Solid red symbols in Figure 3b show the voltage dependence of the photocurrent recorded at the end of the illumination (hereby referred to as saturation current), right before the light is switched off. For potentials below 0 V (vs Ag/AgCl) the saturation photocurrent is almost voltage independent. For positive potentials, however, the saturation photocurrent decreases and becomes even more positive for potentials larger than +180 mV (vs Ag/AgCl). Interestingly, the stronger photocurrent decay during illumination is accompanied by the appearance of a transient current (with positive sign) after the light is switched off (off decay).

DOI: 10.1021/acsami.5b00711
ACS Appl. Mater. Interfaces 2015, 7, 8099−8107

The voltage dependence and the time response of the photocurrent can be explained with the help of the energy diagram shown in Figure 4a by considering the two main electron transfer processes at the electrode/electrolyte interface. The dashed lines represent the possible electron pathways, while the curved arrows correspond to the direction of the cathodic and the anodic currents. At very negative bias potentials (shown by the gray region in the energy diagram of Figure 4a), the negative photocurrent results from the reduction of AMF molecules in solution, which are then oxidized by providing the low energy electron to the P-state of the RCs. The sign of this current is negative (cathodic or reduction current, i_{cat}), i.e., electrons are injected from the electrode to the solution. In addition to this electron transfer process, we also have to consider the possibility of an anodic current (positive, i_{an}) resulting from the oxidation of QH_2 molecules generated during illumination. This current depends on the concentration of the QH_2 present in solution (which is related to the activity of the RCs upon photostimulation) and on the overpotential with respect to the formal potential of the Q_0/QH_2 redox couple, which is about −100 mV vs Ag/AgCl.[40] When the electrode is biased with enough overpotential with respect to this value, QH_2 molecules generated during illumination can be oxidized at the electrode. The anodic current transient observed in the positive bias regime (shown with a red region in the energy diagram of Figure 4a) after the light is switched off (off decay shown in the upper right inset in Figure 3a) is attributed to the oxidation of the excess of photogenerated QH_2 molecules. In fact, this anodic current is also present during illumination and is responsible for the voltage-dependent decay of the photocurrent shown in Figure 3b. At any time t, the measured total photocurrent $i_{ph}^{tot}(t)$ equals the sum of the cathodic and the anodic currents $i_{cat}(t)$ and $i_{an}(t)$. The curves in Figure 3a reveal that an equilibrium situation is reached after about 100 s of illumination; at this equilibrium, which depends on the bias voltage, we can assume a concentration of QH_2 in the electrode's vicinity $[QH_2](U_{bias}, t_{OFF}^-)$, which is responsible for the anodic current $i_{an}(t_{OFF}^-)$, where t_{OFF}^- is the left-hand limit of the time t_{OFF} when the light is switched off. Similarly, (t_{OFF}^+) is defined as the right-hand limit of t_{OFF}. At $t = t_{OFF}^+$, we can assume the same concentration of QH_2 at the surface, and thus $i_{an}(t_{OFF}^-) = i_{an}(t_{OFF}^+)$. In this way, we can use $i_{an}(t_{OFF}^+)$ to calculate the corrected voltage dependence of $i_{cat}(t_{OFF}^-)$; the result of this correction is shown in Figure 3b by the open symbols.

The same analysis has been conducted for the electrodes in which cyt-c was used as electron mediator in solution. Figure 3c shows curves of photocurrent versus time recorded at different bias potentials for the case of cyt-c. Compared to the response of the system with AMF electron mediators, we observe very slow off−on and on−off transitions, as well as a much smaller decay during illumination (on decay). The time response will be discussed in more detail below. Another difference with respect to the experiments with AMF electron mediators is the absence of any transient anodic current after switching off the light (off decay). In order to discuss the voltage dependence of the photocurrent, Figure 3b also shows $i_{ca}(t_{OFF}^-)$ for the experiments with cyt-c electron mediators.

For the experiments with AMF electron mediators, a constant current $i_{cat}(t_{OFF}^-)$ is observed over the explored bias regime (red open symbols in Figure 3b). Provided that there is enough overpotential with respect to the formal potential of the AMF mediator, the electrode can efficiently reduce AMF molecules, which can then provide the electrons to the RCs. Since the formal potential of AMF is at +320 mV vs Ag/AgCl, the biasing of the electrode at potentials below +200 mV vs Ag/AgCl results in a charge transfer already limited by diffusion,[41] which explains why the photocurrent is voltage independent in this bias regime.

In the case of cyt-c mediators, the saturation photocurrent only appears at electrode potentials more negative than the reduction potential of cyt-c, which is about +30 mV vs Ag/AgCl (see Supporting Information). The solid lines in Figure 3b are fits to $i_{cat}(t_{OFF}^-)$ using a current−voltage dependence corresponding to the case of mass transfer limitation by diffusion (details are provided in the Supporting Information), showing a good agreement between experiments and theory.

In order to gain a deeper insight into the mechanism of photocurrent generation, we have investigated the dynamics of the photocurrent. Figure 4b shows the decay of photocurrent during illumination (on decay) in the different bias regimes (−50 mV black curve, +170 mV green curve) as well as the current transition at +170 mV bias (blue curve) after switching off the light (off decay) for the case of AMF mediators in the solution. In the negative bias regime, the on decay can be modeled based on the following considerations: at this negative bias, we can assume that all AMF molecules in the vicinity of the electrode are in the reduced form right before the illumination, i.e., at t_{ON}^-. At t_{ON}^+, the fast electron transfer between RCs and AMF molecules results in a high concentration of oxidized AMF molecules close to the electrode $C_{AMF^{ox}}^*(t_{ON}^+)$. The oxidized AMF can be reduced at the electrode, resulting in the observed photocurrent $i_{cat}(t)$. In a first approximation, $i_{cat}(t)$ is proportional to the time-dependent concentration of oxidized AMF $C_{AMF^{ox}*}(t)$. Considering first-order kinetics, the time dependence of $C_{AMF^{ox}*}(t)$ can be calculated from

$$\frac{dC_{AMF^{ox}}^*(t)}{dt} = -pC_{AMF^{ox}}^*(t) + kC_{AMF^{red}}^*(t) \quad (1)$$

where the first term describes the reduction process at the electrode (governed by the mass transfer rate constant p) and the second term represents the regeneration of oxidized AMF by the RCs (governed by the rate constant k). The analytical solution of this rate equation (a detailed derivation is provided in the Supporting Information) yields the following time dependence of the photocurrent

$$i_{cat}(t) = a + b\cdot\exp\left[-p\left(1 + \frac{k}{p}\right)t\right] \quad (2)$$

The curve labeled "Fit 1" in Figure 4b represents the fit (using eq 2) of the on decay recorded at a bias of −50 mV vs Ag/AgCl, showing a very good agreement for $t > 1$ s.

At +170 mV vs Ag/AgCl, the on decay exhibits a time dependence characteristic of a diffusion-limited process.[41] As explained above, the photocurrent decay in this bias regime (green curve) is dominated by the oxidation of the QH_2 molecules at the electrode. After the light is switched off, the decay of the anodic current (off decay, blue curve) has the same origin and exhibits the same time dependence, if we consider the absolute value. This oxidation process can be adequately described by the diffusion-limited current represented by the Cottrell equation, in which $i(t) \propto 1/\sqrt{t}$ (see curve "Fit 2" in Figure 4a).

DOI: 10.1021/acsami.5b00711
ACS Appl. Mater. Interfaces 2015, 7, 8099−8107

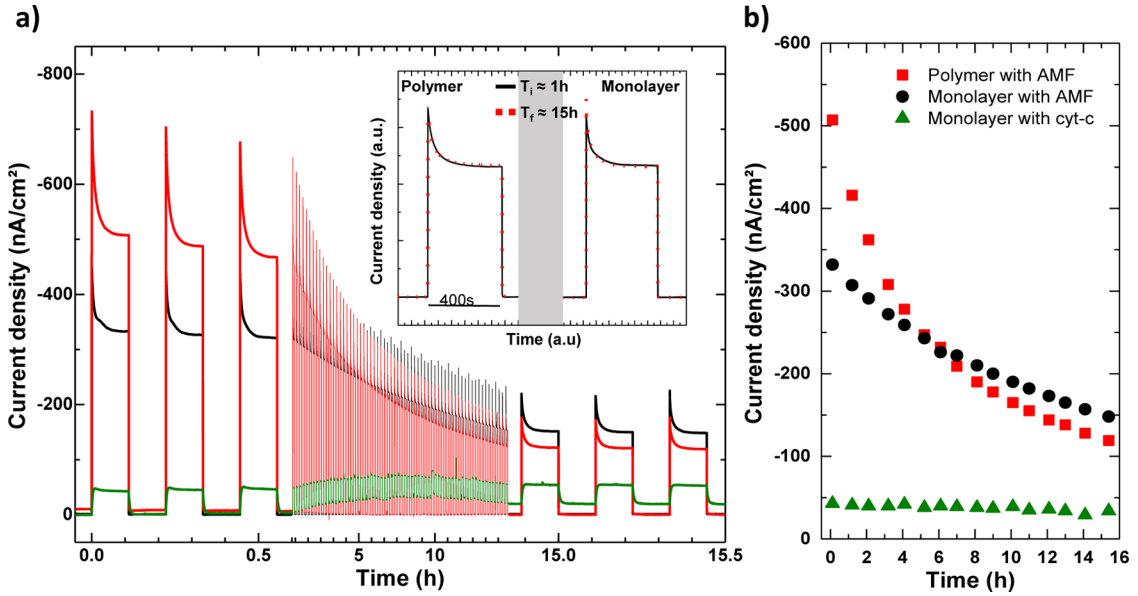

Figure 5. (a) Long-term measurements showing the response of the three different diamond electrodes with physisorbed RC. All measurements are performed in 10 mM PBS buffer with 100 μM Q_0 and the presence of an additional mediator. The green curve represents the sample modified with ML and cytochrome *c* in solution, the black curve corresponds to the combination of ML and AMF in solution, and red represents the polymeric brush-modified electrode with AMF in solution. The IR-LED was switched on and off every 400 s continuously for more than 15 h. The inset shows the comparison of an off/on/off cycle recorded after 1 h (black solid curves) of operation and after 15 h (dashed red curves) for the sample modified with a polymer (left side) and one modified with the ML of 6-phosphonohexanoic acid (right side) normalized by a suitable factor to overlap the two curves. (b) Saturation current density as a function of time for the three different electrodes.

In Figure 4c we show the off−on and on−off transitions of the current for the case of cyt-c electron mediators. As representative examples, the experimental curves recorded at −50 mV (red curves) and +50 mV (gray curves) and their corresponding fits are shown. The observed time dependence of these current transitions can be explained assuming that the charge exchange between cyt-c and the RCs is characterized by a kinetics much slower than the one offered by AMF (see Supporting Information). In this case, the second term on the right-hand side of eq 1 can be neglected. Additionally, this condition also implies that right after the illumination starts (at $t = t^{+}_{ON}$), the concentration of oxidized cyt-c molecules is negligible, $C^{*}_{cyt-c}(t^{+}_{ON}) = 0$. With these boundary conditions, the solution of eq 1 for the off−on transition is given by $i(t) = i(t = \infty)[1 - \exp(-p \cdot t)]$. The on−off transition can be modeled in the same way with the concentration of cyt-c $C^{*}_{cyt-c}(t^{+}_{OFF})$ having a certain value different from zero and depending on the bias voltage. As a result, the on−off transition can be described by $i(t) = i(t = t^{+}_{OFF}) \exp(-p \cdot t)$. More details are provided in the Supporting Information.

Stability Assessment. Finally, we have also investigated the stability of photocurrent generation. Figure 5a shows the results of a long-time photocurrent experiment (over 15 h) for the three different types of devices reported in this study. The value of the saturation current is plotted over time in Figure 5b. The system consisting of the RCs on the ML using cyt-c as the electron mediator exhibits a quite stable but also comparatively small photocurrent. In the case of RCs on the ML but with AMF as electron mediator, the initial photocurrent is high, but after 15 h of operation the photocurrent has decreased to around 30% of its initial value. This value is comparable with the decrease observed from den Hollander et al. after 13 h of operation.[9] The performance of RCs-based biophotovoltaic electrodes in terms of photocurrent density over long operational time is not presented in most of the relevant literature where the photocurrent measurements are limited to the scale of seconds. For the experiment with the RCs confined in the polymer brushes and using AMF electron mediators, the very high initial photocurrent also exhibits the fastest degradation with time. Although the polymer brushes seem to offer an advantage in terms of the number of RCs which can be loaded on the electrode, our experiments suggest that they exhibit an inferior stability compared to the system modified with 6-phosphonohexanoic acid.

In the inset of Figure 5a, we compare an off/on/off cycle recorded after 1 h of operation (black solid curve) with a cycle recorded after 15 h of operation (red dashed curve). The curves are normalized to facilitate the comparison. As is clear from the good overlap of the two curves, both for the case of polymers modified electrode (left side) and for the monolayer (right side), the on decay remains unchanged. The dynamics of the photocurrent generation mechanism seems to be the same over the 15 h of operation, even though the absolute current decreases. Considering that the concentration of electron mediators in solution is not significantly modified during the course of the experiment (see Supporting Information), we can thus attribute the decrease of absolute photocurrent over time to the degeneration or desorption of active RCs from the electrode. The reason the rate of degradation is different for the different samples (as shown in Figure 5b) is a complex issue. It can be related to a degradation of the polymeric brush itself or to the stability of the interaction between the RCs and the functional groups on the polymer rather than on the monolayer.

CONCLUSION

We reported on the realization of a biophotovoltaic hybrid system consisting of RCs from purple bacteria immobilized on different functional nanocrystalline conductive diamond elec-

DOI: 10.1021/acsami.5b00711
ACS Appl. Mater. Interfaces 2015, 7, 8099−8107

trodes. Using the functionalized diamond electrodes and the photoreactive RCs as building blocks for a simple biosolar cell, our work demonstrates a route to increase the loading of photoreactive units by tailoring the electrode surface with polymer brushes, yielding an enhancement of the photocurrent. This has been possible through the employment of diamond: this material, used here for the first time in RCs based biohybrid systems, is a versatile platform for different functionalization methods thanks to the well-known carbon chemistry. In addition, based on an electrochemical study of the charge transfer between different redox species and their role in the production of photocurrent, we report on the use of a novel electron mediator, aminomethyl ferrocene, leading to an enhanced photocurrent stable over many hours of operation. Finally, with the help of the equations used to fit the experimental data, we clarify the mechanisms involved in the different phases of the photocurrent generation for several electrode designs. This model can be used as a proof of concept to describe more complex or different systems based on RCs integrated on an electrode.

■ ASSOCIATED CONTENT

Ⓢ Supporting Information

Detailed description of the diamond functionalization methods used. Basic electrochemical characterization of diamond electrodes with AMF and cyt-c. Photocurrent as a function of the concentration of charge carriers in solution. Analytical derivation of the equations discussed in the main text. Proof of the degradation of RCs after treatment with SDS. This material is available free of charge via the Internet at http://pubs.acs.org.

■ AUTHOR INFORMATION

Corresponding Author

*E-mail: garrido@wsi.tum.de.

Author Contributions

The manuscript was written through contributions of all authors. All authors have given approval to the final version of the manuscript.

Notes

The authors declare no competing financial interest.

■ ACKNOWLEDGMENTS

This project has been funded by the European Union under the NeuroCare FP7 project (grant agreement 280433), the European FP7 Marie Curie Initial Training Network MATCON, the COST Action TD1102 (Photosynthetic proteins for technological application: biosensors and biochips), The Deutsche Forschungsgemeinschaft, the Nanosystem Initiative Munich, the Research Foundation Flanders (FWO) (G.0555.10N). Authors would also like to acknowledge Dr. L.H. Hess for his valuable comments.

■ REFERENCES

(1) Janzen, A. F.; Seibert, M. Photoelectrochemical Conversion Using Reaction-Centre Electrodes. *Nature* **1980**, *286*, 584−585.

(2) Das, R.; Kiley, P. J.; Segal, M.; Norville, J.; Yu, A. A.; Wang, L.; Trammell, S. A.; Reddick, L. E.; Kumar, R.; Stellacci, F.; Lebedev, N.; Schnur, J.; Bruce, B. D.; Zhang, S.; Baldo, M. Integration of Photosynthetic Protein Molecular Complexes in Solid-State Electronic Devices. *Nano Lett.* **2004**, *4*, 1079−1083.

(3) Carmeli, I.; Frolov, L.; Carmeli, C.; Richter, S. Photovoltaic Activity of Photosystem I-Based Self-Assembled Monolayer. *J. Am. Chem. Soc.* **2007**, *129*, 12352−12353.

(4) Trammell, S.; Griva, I.; Spano, A.; Tsoi, S.; Tender, L.; Schnur, J.; Lebedev, N. Effects of Distance and Driving Force on Photoinduced Electron Transfer between Photosynthetic Reaction Centers and Gold Electrodes. *J. Phys. Chem. C* **2007**, *111*, 17122−17130.

(5) Lebedev, N.; Trammell, S. A.; Tsoi, S.; Spano, A.; Kim, J. H.; Xu, J.; Twigg, M. E.; Schnur, J. M. Increasing Efficiency of Photoelectronic Conversion by Encapsulation of Photosynthetic Reaction Center Proteins in Arrayed Carbon Nanotube Electrode. *Langmuir* **2008**, *24*, 8871−8876.

(6) Ham, M.-H.; Choi, J. H.; Boghossian, A. A.; Jeng, E. S.; Graff, R. A.; Heller, D. A.; Chang, A. C.; Mattis, A.; Bayburt, T. H.; Grinkova, Y. V.; Zeiger, A. S.; Van Vliet, K. J.; Hobbie, E. K.; Sligar, S. G.; Wraight, C. A.; Strano, M. S. Photoelectrochemical Complexes for Solar Energy Conversion that Chemically and Autonomously Regenerate. *Nat. Chem.* **2010**, *2*, 929−936.

(7) Ciesielski, P. N.; Faulkner, C. J.; Irwin, M. T.; Gregory, J. M.; Tolk, N. H.; Cliffel, D. E.; Jennings, G. K. Enhanced Photocurrent Production by Photosystem I Multilayer Assemblies. *Adv. Funct. Mater.* **2010**, *20*, 4048−4054.

(8) Badura, A.; Guschin, D.; Kothe, T.; Kopczak, M. J.; Schuhmann, W.; Rögner, M. Photocurrent Generation by Photosystem 1 Integrated in Crosslinked Redox Hydrogels. *Energy Environ. Sci.* **2011**, *4*, 2435.

(9) den Hollander, M.-J.; Magis, J. G.; Fuchsenberger, P.; Aartsma, T. J.; Jones, M. R.; Frese, R. N. Enhanced Photocurrent Generation by Photosynthetic Bacterial Reaction Centers through Molecular Relays, Light-harvesting Complexes, and Direct Protein-Gold Interactions. *Langmuir* **2011**, *27*, 10282−10294.

(10) Kondo, M.; Iida, K.; Dewa, T.; Tanaka, H.; Ogawa, T.; Nagashima, S.; Nagashima, K. V. P.; Shimada, K.; Hashimoto, H.; Gardiner, A. T.; Cogdell, R. J.; Nango, M. Photocurrent and Electronic Activities of Oriented-His-Tagged Photosynthetic Light-harvesting/Reaction Center Core Complexes Assembled onto a Gold Electrode. *Biomacromolecules* **2012**, *13*, 432−438.

(11) Yehezkeli, O.; Tel-Vered, R.; Wasserman, J.; Trifonov, A.; Michaeli, D.; Nechushtai, R.; Willner, I. Integrated Photosystem II-Based Photo-Bioelectrochemical Cells. *Nat. Commun.* **2012**, *3*, 742.

(12) Gunther, D.; LeBlanc, G.; Prasai, D.; Zhang, J. R.; Cliffel, D. E.; Bolotin, K. I.; Jennings, G. K. Photosystem I on Graphene as a Highly Transparent, Photoactive Electrode. *Langmuir* **2013**, *29*, 4177−4180.

(13) Darby, E.; LeBlanc, G.; Gizzie, E. A.; Winter, K. M.; Jennings, G. K.; Cliffel, D. E. Photoactive Films of Photosystem I on Transparent Reduced Graphene Oxide Electrodes. *Langmuir* **2014**, *30*, 8990−8994.

(14) Carmeli, I.; Mangold, M.; Frolov, L.; Zebli, B.; Carmeli, C.; Richter, S.; Holleitner, A. W. A Photosynthetic Reaction Center Covalently Bound to Carbon Nanotubes. *Adv. Mater.* **2007**, *19*, 3901−3905.

(15) Yehezkeli, O.; Tel-Vered, R.; Michaeli, D.; Willner, I.; Nechushtai, R. Photosynthetic Reaction Center-Functionalized Electrodes for Photo-Bioelectrochemical Cells. *Photosynth. Res.* **2014**, *120*, 71−85.

(16) Kamran, M.; Delgado, J. D.; Friebe, V.; Aartsma, T. J.; Frese, R. N. Photosynthetic Protein Complexes as Bio-Photovoltaic Building Blocks Retaining a High Internal Quantum Efficiency. *Biomacromolecules* **2014**, *15*, 2833−2838.

(17) Mahmoudzadeh, A.; Saer, R.; Jun, D.; Mirvakili, S. M.; Takshi, A.; Iranpour, B.; Ouellet, E.; Lagally, E. T.; Madden, J. D. W.; Beatty, J. T. Photocurrent Generation by Direct Electron Transfer using Photosynthetic Reaction Centres. *Smart Mater. Struct.* **2011**, *20*, 094019.

(18) Okamura, M. Y.; Feher, G. Proton Transfer in Reaction Centers from Photosynthetic Bacteria. *Annu. Rev. Biochem.* **1992**, *61*, 861−896.

(19) Okamura, M. Y.; Paddock, M.; Graige, M.; Feher, G. Proton and Electron Transfer in Bacterial Reaction Centers. *Biochim. Biophys. Acta, Bioenerg.* **2000**, *1458*, 148−163.

(20) Stowell, M. H. Light-Induced Structural Changes in Photosynthetic Reaction Center: Implications for Mechanism of Electron-Proton Transfer. *Science* **1997**, *276*, 812−816.

DOI: 10.1021/acsami.5b00711
ACS Appl. Mater. Interfaces 2015, 7, 8099−8107

(21) Kirmaier, C.; Holten, D. Primary Photochemistry of Reaction Centers from the Photosynthetic Purple Bacteria. *Photosynth. Res.* **1987**, *13*, 225−260.
(22) Parson, W. W.; Warshel, A. Mechanism of Charge Separation in Purple Bacterial Reaction Centers. *Adv. Photosynth. Respir.* **2009**, *28*, 355−377.
(23) Trammell, S. A.; Wang, L.; Zullo, J. M.; Shashidhar, R.; Lebedev, N. Orientated Binding of Photosynthetic Reaction Centers on Gold using NiNTA Self-assembled Monolayers. *Biosens. Bioelectron.* **2004**, *19*, 1649−1655.
(24) Trammell, S. A.; Spano, A.; Price, R.; Lebedev, N. Effect of Protein Orientation on Electron Transfer between Photosynthetic Reaction Centers and Carbon Electrodes. *Biosens. Bioelectron.* **2006**, *21*, 1023−1028.
(25) Lebedev, N.; Trammell, S. A.; Spano, A.; Lukashev, E.; Griva, I.; Schnur, J. Conductive Wiring of Immobilized Photosynthetic Reaction Center to Electrode by Cytochrome c. *J. Am. Chem. Soc.* **2006**, *128*, 12044−12045.
(26) Manocchi, A. K.; Baker, D. R.; Pendley, S. S.; Nguyen, K.; Hurley, M. M.; Bruce, B. D.; Sumner, J. J.; Lundgren, C. A. Photocurrent Generation from Surface Assembled Photosystem I on Alkanethiol Modified Electrodes. *Langmuir* **2013**, *29*, 2412−2419.
(27) Stavis, C.; Clare, T. L.; Butler, J. E.; Radadia, A. D.; Carr, R.; Zeng, H.; King, W. P.; Carlisle, J. A.; Aksimentiev, A.; Bashir, R.; Hamers, R. J. Surface Functionalization of Thin-film Diamond for Highly Stable and Selective Biological Interfaces. *Proc. Natl. Acad. Sci. U. S. A.* **2011**, *108*, 983−988.
(28) Strother, T.; Knickerbocker, T.; Russell, J. N.; Butler, J. E.; Smith, L. M.; Hamers, R. J. Photochemical Functionalization of Diamond Films. *Langmuir* **2002**, *18*, 968−971.
(29) Caterino, R.; Csiki, R.; Wiesinger, M.; Sachsenhauser, M.; Stutzmann, M.; Garrido, J. A.; Cattani-Scholz, A.; Speranza, G.; Janssens, S. D.; Haenen, K. Organophosphonate Biofunctionalization of Diamond Electrodes. *ACS Appl. Mater. Interfaces* **2014**, *6*, 13909−13916.
(30) Hutter, N. A.; Steenackers, M.; Reitinger, A.; Williams, O. A.; Garrido, J. A.; Jordan, R. Nanostructured Polymer Brushes and Protein Density Gradients on Diamond by Carbon Templating. *Soft Matter* **2011**, *7*, 4861.
(31) Reitinger, A. A.; Hutter, N. A.; Donner, A.; Steenackers, M.; Williams, O. A.; Stutzmann, M.; Jordan, R.; Garrido, J. A. Functional Polymer Brushes on Diamond as a Platform for Immobilization and Electrical Wiring of Biomolecules. *Adv. Funct. Mater.* **2013**, *23*, 2979−2986.
(32) Yaghoubi, H.; Li, Z.; Jun, D.; Saer, R.; Slota, J. E.; Beerbom, M.; Schlaf, R.; Madden, J. D.; Beatty, J. T.; Takshi, A. The Role of Gold-Adsorbed Photosynthetic Reaction Centers and Redox Mediators in the Charge Transfer and Photocurrent Generation in a Bio-Photoelectrochemical Cell. *J. Phys. Chem. C* **2012**, *116*, 24868−24877.
(33) Lancaster, C. R. D.; Michel, H. *Photosynthetic Reaction Centers of Purple Bacteria*; John Wiley & Sons: Chichester, 2001.
(34) Subramanian, P.; Motorina, A.; Yeap, W. S.; Haenen, K.; Coffinier, Y.; Zaitsev, V.; Niedziolka-Jonsson, J.; Boukherroub, R.; Szunerits, S. An Impedimetric Immunosensor Based on Diamond Nanowires Decorated with Nickel Nanoparticles. *Analyst* **2014**, *139*, 1726.
(35) Yeap, W. S.; Liu, X.; Bevk, D.; Pasquarelli, A.; Lutsen, L.; Fahlman, M.; Maes, W.; Haenen, K. Functionalization of Boron-Doped Nanocrystalline Diamond with N3 Dye Molecules. *ACS Appl. Mater. Interfaces* **2014**, *6*, 10322−10329.
(36) Janssens, S. D.; Pobedinskas, P.; Vacik, J.; Petráková, V.; Ruttens, B.; D'Haen, J.; Nesládek, M.; Haenen, K.; Wagner, P. Separation of Intra- and Intergranular Magnetotransport Properties in Nanocrystalline Diamond Films on the Metallic Side of the Metal−Insulator Transition. *New J. Phys.* **2011**, *13*, 083008.
(37) Hermanson, G. T. *Bioconjugate Techniques*, 2nd ed; Academic Press: San Diego, 1996.
(38) Granger, M. C.; Witek, M.; Xu, J.; Wang, J.; Hupert, M.; Hanks, A.; Koppang, M. D.; Butler, J. E.; Lucazeau, G.; Mermoux, M.; Strojek, J. W.; Swain, G. M. Standard Electrochemical Behavior of High-Quality, Boron-Doped Polycrystalline Diamond Thin-Film Electrodes. *Anal. Chem.* **2000**, *72*, 3793−3804.
(39) Yaghoubi, H.; Li, Z.; Jun, D.; Lafalce, E.; Jiang, X.; Schlaf, R.; Beatty, J. T.; Takshi, A. Hybrid Wiring of the Rhodobacter sphaeroides Reaction Center for Applications in Bio-photoelectrochemical Solar Cells. *J. Phys. Chem. C* **2014**, *118*, 23509−23518.
(40) Dryhurst, G. *Biological Electrochemistry*, *1*st ed.; Academic Press: New York, 1982.
(41) Bard, A. J.; Faulkner, L. R. *Electrochemical methods and applications*, 2nd ed; Wiley-Interscience: New York, London, 2000.

DOI: 10.1021/acsami.5b00711
ACS Appl. Mater. Interfaces 2015, 7, 8099−8107